

Report for exercise 3 from group K

Tasks addressed: 5

Authors: SONJA KRAFFT (03681252)

LUDWIG-FERDINAND STUMPP (03736583)

TIMUR WOHLLEBER (03742932)

Last compiled: 2021-12-08

Source code: <https://gitlab.lrz.de/00000000014A9334/mlcs-ex3-bifurcation-and-visualization>

The work on tasks was divided in the following way:

SONJA KRAFFT (03681252)	Task 1	33%
	Task 2	33%
	Task 3	33%
	Task 4	33%
	Task 5	33%
LUDWIG-FERDINAND STUMPP (03736583)	Task 1	33%
	Task 2	33%
	Task 3	33%
	Task 4	33%
	Task 5	33%
TIMUR WOHLLEBER (03742932)	Task 1	33%
	Task 2	33%
	Task 3	33%
	Task 4	33%
	Task 5	33%

1 Introduction

Goal of this exercise

Dynamic systems in practice are often dependent on a variety of parameters. The influence of these parameters significantly determines the behaviour of these systems and must therefore be taken into account in the development and design of models. Due to this urgency, this task intends to provide a general overview of both the mathematical principles and possible analysis methods such as the evaluation of orbits and bifurcation diagrams for non-linear systems. Furthermore, this task serves to familiarise with the concept of chaos and to understand the dependence of initial conditions and system parameters. Beyond that, the practical relevance of stability points and bifurcations in real scenarios is demonstrated using the SIR model.

Python dependencies

Due to the great selection of publicly available libraries, *Python* is chosen as the programming language for this exercise. The following is a listing of required software and *Python* packages in order to run and maintain the code.

For plotting, we use both *matplotlib.pyplot*, as well as the built on top *seaborn* library that works nicely together with *pandas.DataFrame*. *SciPy* and *NumPy* are used for the core mathematical simulations, where especially the solvers of *Scipy* are of great value for solving differential equations.

We use *JupyterLab* for prototyping and analysis, *black* for style formatting and *mypy* for static typing. These make up our development dependencies, only needed to run and develop the code, not necessarily dependencies of the internal codebase.

python	3.9.5
vscode	1.62.3

Table 1: Python version and code editor.

matplotlib	3.4.3
numpy	1.21.3
pandas	1.3.4
seaborn	0.11.2
scipy	1.7.1

Table 2: List of required *Python* packages to run the code of the repository. Find the corresponding `requirements.txt` file inside the root of the directory.

mypy	0.910
black	21.11b1
jupyterlab	3.2.1

Table 3: List of development dependencies in order to develop the code and make adjustments. Find the corresponding `requirements-dev.txt` file inside the root of the directory.

2 Individual Tasks

Report on task 1/5: Vector fields, orbits, and visualization

Notebook: `task_1.ipynb`

Code: `helpers/math.py`, `helpers/plots.py`

Motivation

This subsection is concerned with analysing a first simple, parameterisable, dynamical system. We look at the resulting phase portraits for given parameterisations and evaluate their topological equivalence.

Defining a simple linear dynamical system

In the following, we consider a general linear dynamical system with state space $X = \mathbb{R}^2$ and an index set in continuous time $I = \mathbb{R}$. The derivative of the evolution operator ϕ with respect to time t is given into:

$$\frac{d\phi(t, \mathbf{x})}{dt} \Big|_{t=0} = A\mathbf{x} \quad (1)$$

where $A \in \mathbb{R}^{2 \times 2}$ is a general parameterised, squared matrix:

$$A = \begin{bmatrix} \alpha & \beta \\ \gamma & \delta \end{bmatrix} \quad (2)$$

Writing out the matrix multiplication, one can decompose the vector representation as:

$$\frac{d\phi(t, x_1)}{dt} \Big|_{t=0} = \alpha x_1 + \beta x_2 \quad (3)$$

$$\frac{d\phi(t, x_2)}{dt} \Big|_{t=0} = \gamma x_1 + \delta x_2 \quad (4)$$

Analysis: Stabilities, eigenvalues, phase portraits

Using the defined linear dynamical system (1), we observe its stability based on different matrices A . Table 4 shows the topological classification of the resulting hyperbolic equilibria on the plane.

Reasoning about local topological equivalence

First, one can prove that the shown types of phase portraits can be divided into three locally different topological classes around their equilibria depending on the number of eigenvalues with a positive or negative real value.

Theorem 1 from Kuznetsov [4, p.48] proves this condition as sufficient to classify the topological classes locally apart from each other.

Theorem 1. “The phase portraits of system(s) (...) near two hyperbolic equilibria, x_0 and y_0 , are locally topologically equivalent if and only if these equilibria have the same number n_- and n_+ of eigenvalues with $\text{Re } \lambda < 0$ and with $\text{Re } \lambda > 0$, respectively.” [4, p.48].

Following the argumentation of Kuznetsov [4, p.48], this theorem is a combination of two sub-parts:

1. *Linearisation*: According to the *Grobman-Hartman Theorem*, there exists a locally topologically equivalent linearisation at the point of the equilibrium that can be applied to the equilibrium points of both to be compared systems.
2. *Equivalence of linear systems*: Two linear systems are topologically equivalent if they have the same number of eigenvalues with positive and negative real parts and no exclusively imaginary eigenvalues.

If we apply Theorem 1 to the observed equilibria on the plane, we can divide the listed cases into three local topological classes by looking at the real part of the eigenvalues (see table 4):

1. stable nodes / foci: Two eigenvalues with a negative real part.
2. unstable saddles: One eigenvalue with a positive, one eigenvalue with a negative real part.
3. unstable nodes / foci: Two eigenvalues with a positive real part.

Reasoning about general topological equivalence

Since the three listed classes are not even locally topologically equivalent around their equilibria, they cannot be topologically equivalent in general either.

Note that within one of these topological classes, nodes and foci are topologically equivalent, since there exists a homeomorphism that maps orbits of the first system into orbits of the second system (compare to example 2.1 in Kuznetsov [4, p.43]).

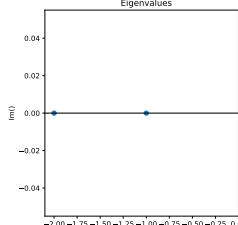
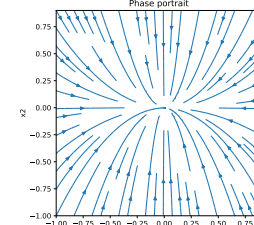
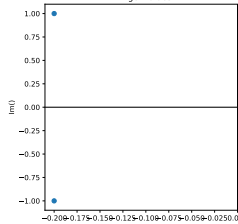
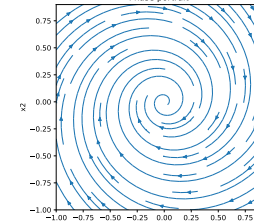
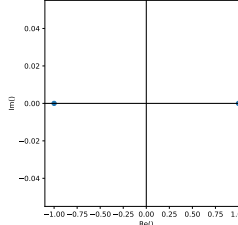
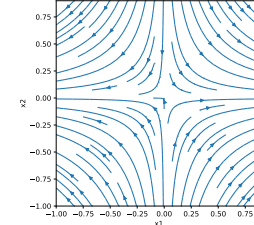
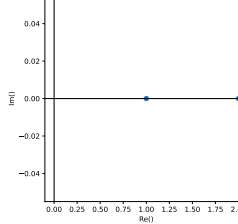
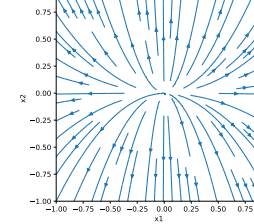
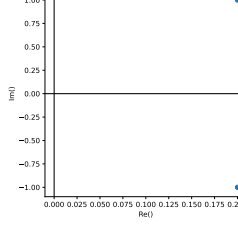
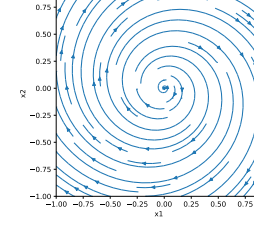
(n_+, n_-)	Matrix A	Eigenvalues	Phase portrait	Type	Stability
$(0, 2)$	$A = \begin{bmatrix} -1 & 0 \\ 0 & -2 \end{bmatrix}$			node	stable
	$A = \begin{bmatrix} -0.2 & 1 \\ -1 & -0.2 \end{bmatrix}$			focus	
$(1, 1)$	$A = \begin{bmatrix} 1 & 0 \\ 0 & -1 \end{bmatrix}$			saddle	unstable
$(2, 0)$	$A = \begin{bmatrix} 1 & 0 \\ 0 & 2 \end{bmatrix}$			node	unstable
	$A = \begin{bmatrix} 0.2 & 1 \\ -1 & 0.2 \end{bmatrix}$			focus	

Table 4: Topological classification of hyperbolic equilibria on the plane of an observed linear dynamical system $\dot{\mathbf{x}} = A\mathbf{x}$. Topological classes are separated with a horizontal line based on the number of eigenvalues with a positive and negative real value part. Table is inspired by Kuznetsov [4, p.49].

Report on task 2/5: Common bifurcations in nonlinear systems

Notebook: `task_2.ipynb`

Code: `helpers/math.py`, `helpers/plots.py`

Motivation

In this task, we are interested in analysing a simple bifurcation by considering the resulting steady states for a given parameterisation. We then compare two quantitatively different dynamical systems regarding topological equivalences for given parameter configurations and conclude on their normal form.

Defining a one-dimensional quadratic dynamical system

First, we analyze the bifurcation of a one-dimensional quadratic dynamical system with one-dimensional state $x \in \mathbb{R}$ and continuous time $t \in \mathbb{R}$. The evolution over time is defined as:

$$\dot{x} = \alpha - x^2 \quad (5)$$

where the parameter α defines a constant offset for the evolution.

In order to analyse the steady states of the given system, one can set $\dot{x} = 0$ and solve for states x that fulfil this equation, based on the parameter α . Due to the quadratic nature of the evolution, one can observe three different cases:

$$x_{\dot{x}=0}(\alpha) = \begin{cases} \emptyset & \alpha < 0 \\ 0 & \alpha = 0 \\ \pm\sqrt{\alpha} & \alpha > 0 \end{cases} \quad (6)$$

The number of steady states depends on the value of our parameter α and can either take the value zero, one, or two, as depicted in equation (6). Around the parameter value $\alpha = 0$, the topology of the system changes from "no steady states" to "two steady states". This bifurcation at $\alpha = 0$ is known as the *saddle-node bifurcation* with its normal form:

$$\dot{x} = r - x^2 \quad (7)$$

The number of steady states and their stability, both depending on the value of the parameter α , are visualized in figure 1a. The figure has been created by defining a equidistant vector of 100 values of α between the interval $-2 < \alpha < 2$ and checking the number and type of stability points for each single value. The bifurcation point is shown with a black vertical line and is happening for $\alpha = 0$.

Comparison to another one-dimensional quadratic dynamical system

Now, we compare our first dynamical system (5) with another similar system of the evolution:

$$\dot{x} = \alpha - 2x^2 - 3 \quad (8)$$

Figure 1b shows the results of the same stability analysis as described before. Here, one can see that both systems seem to follow the same bifurcation, namely a *saddle-node-bifurcation*. Whereas for the first system the bifurcation happens at $\alpha = 0$, this time it happens at $\alpha = 3$.

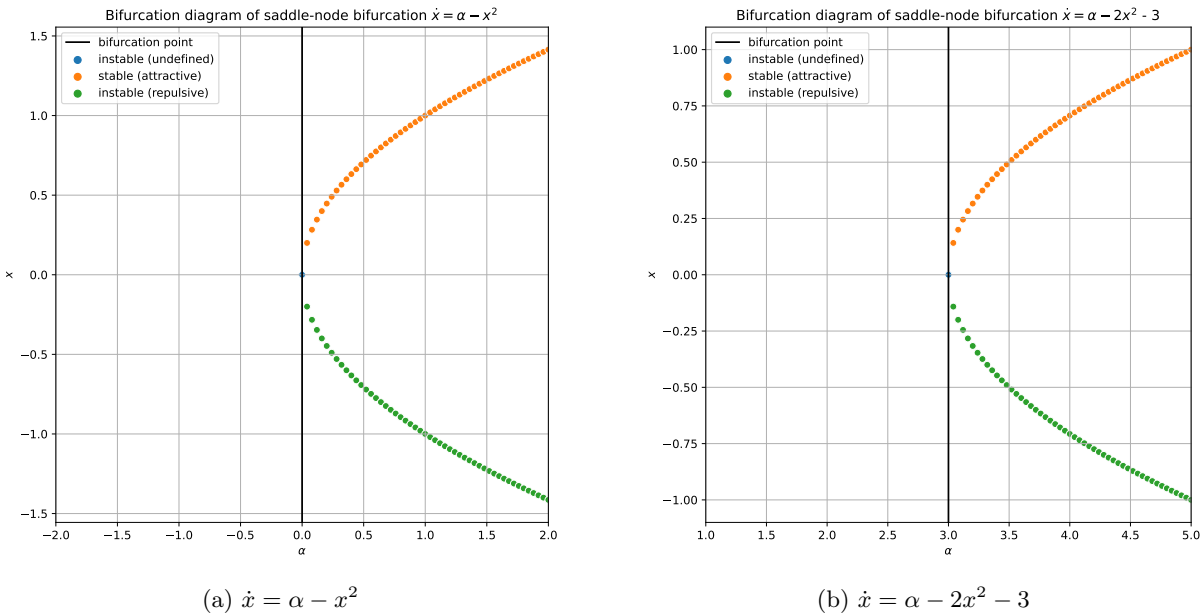


Figure 1: Bifurcation diagrams of two *saddle-node bifurcations*. Shown are equilibrium points, tested with a step size of $\Delta\alpha = 0.04$ and colored depending on their stability. The parameter value α for the bifurcation point is visualised with a black vertical line. The stability is tested numerically by looking at points close to both sides of the observed steady state.

Checking for topological equivalence at given configurations

Although the systems are quantitatively different, one can compare the topology of both systems at given parameter values α and check for topological equivalence:

	α	# of steady states
$\dot{x} = \alpha - x^2$	1	2
	-1	0
$\dot{x} = \alpha - 2x^2 - 3$	1	0
	-1	0

Table 5: Number of steady states at given values for parameter α for two quadratic dynamical systems. Results are in alignment to figure 1.

For $\alpha = 1$, the number of steady states is different in both systems. This is why there cannot be a homeomorphism that maps from one system of orbits to the other. Since this is a necessary condition for topological equivalence, the resulting systems at $\alpha = 0$ are not topologically equivalent. For the parameter value $\alpha = -1$ however, both systems do not have any steady state, which is why there exists a homeomorphism mapping from one system to the other. Therefore, both resulting systems are considered topologically equivalent at this parameter configuration.

Comparing the normal forms of both systems

While the systems are provably not topologically equivalent for all parameter values α , they do have the same normal form (independent of the parameter α , they can be mapped to the same system) which is given by the *saddle-node bifurcation* as:

$$\dot{x} = r - x^2 \tag{9}$$

The first system $\dot{x} = \alpha - x^2$ (5) is the same as above normal form (9) by replacing *alpha* with r . The second system $\dot{x} = \alpha - 2x^2 - 3$ (8) also has the same normal form since:

1. One can replace *alpha* – 3 with r .
2. At the point $(x, r) = (0, 0)$ the system $f(x, r) = \frac{dx}{dt} = r - 2x^2$ has a first derivative $\frac{df}{dx}\Big|_{x=0, r=0} = 0$, matching the normal form, while the second derivative $\frac{d^2 f}{dx^2}\Big|_{x=0, r=0} = -4 \neq 0$ (*nondegeneracy condition*) as well as $\frac{df}{dr}\Big|_{x=0, r=0} = 1 \neq 0$ (*transversality condition*).

The second part of this argumentation is originally described in [1] and uses parts of Kuznetsov [4].

Report on task 3/5: Bifurcations in higher dimensions

Notebook: `task_3.ipynb`

Code: `helpers/math.py`, `helpers/plots.py`

Motivation

In the previous sections, we have been dealing with dynamical systems with a one-dimensional state space and a one-dimensional parameter. However, bifurcations can also appear in higher dimensions.

Andronov-Hopf bifurcation

Mathematical description

The *Andronov-Hopf bifurcation* is described by its normal form:

$$\begin{aligned}\dot{x}_1 &= \alpha x_1 - x_2 - x_1(x_1^2 + x_2^2) \\ \dot{x}_2 &= x_1 + \alpha x_2 - x_2(x_1^2 + x_2^2)\end{aligned}\tag{10}$$

There is a two-dimensional state space $x \in \mathbb{R}^2$, a continuous time space $t \in \mathbb{R}$ and one free parameter $\alpha \in \mathbb{R}$.

Visualizing the bifurcation

In order to analyze the bifurcation, we take a look at the resulting phase plots for given values of the parameter α , as shown in figure 2. For values of $\alpha < 0$, there exists one attractive steady state at $\mathbf{x} = (0, 0)$ (figure 2a). For $\alpha > 0$, there is one repulsive steady state at $\mathbf{x} = (0, 0)$ and one attracting limit cycle with growing radius for increasing values of α (figure 2c). The bifurcation is happening at $\alpha = 0$ and bifurcates the system from one topological state into the other (figure 2b).

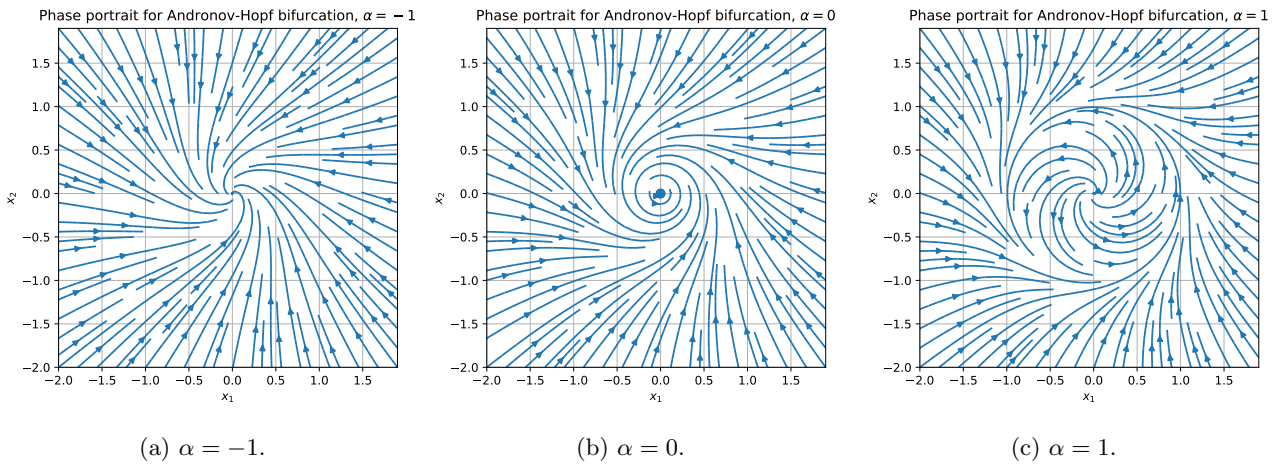


Figure 2: Phase diagrams of the *Andronov-Hopf bifurcation* for varying values of the parameter α with bifurcation at $\alpha = 0$. Phase diagrams show the vector field given the two dimensional state space $(x_1, x_2) \in \mathbb{R}^2$. At the bifurcation point at $\alpha = 0$ (b), the steady state at $\mathbf{x} = (0, 0)$ (a) bifurcates into one attracting limit cycle with growing radius and one repulsive steady state at $\mathbf{x} = (0, 0)$ (c).

Visualizing orbits at a given parameter configuration

In order to analyze the behaviour of a dynamical system, one can plot the orbit given a configuration of the dynamical system and a starting point $\mathbf{x}_0(t=0)$.

In order to determine the sequence of state spaces that define the orbit, one first needs to solve the initial value problem of the ordinary differential equation provided by the normal form. The python package *SciPy*¹ provides a method *scipy.integrate.odeint*² that use the numerical *lsoda* solver from the *FORTRAN* library *odepack*³. For a more in-depth explanation and analysis of numerical integration methods for ODE models, see [6].

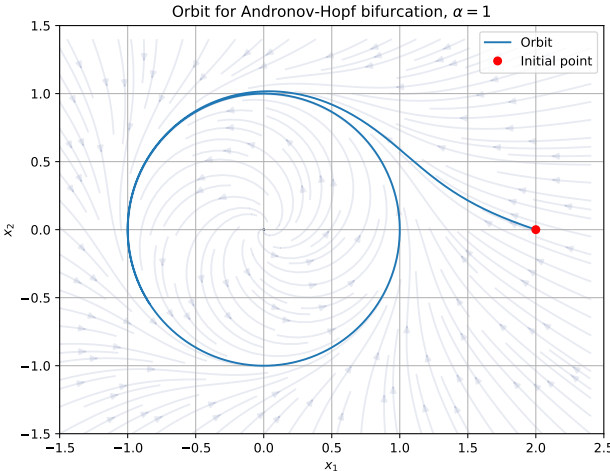
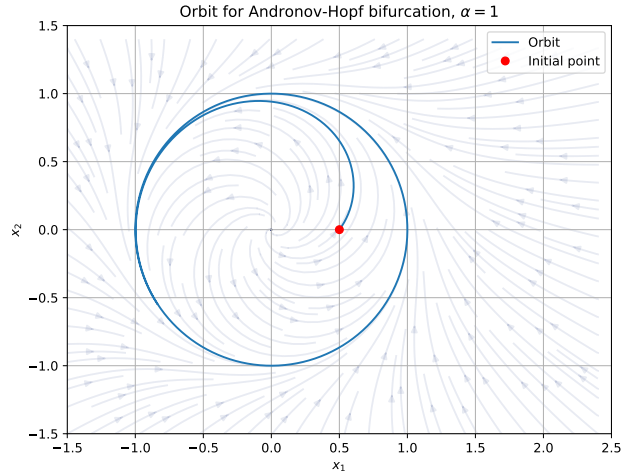
(a) $\mathbf{x}_0 = (2, 0)$.(b) $\mathbf{x}_0 = (0.5, 0)$.

Figure 3: Two orbits of the *Andronov-Hopf* system (10) for $\alpha = 1$, starting at two different initial states, forward in time. In addition to the orbits, the underlying phase plots are shown. As expected, the orbit is following the underlying flow vectors.

Cusp bifurcation

Mathematical description

The *Cusp bifurcation* is another example of a bifurcation in higher dimensions. It has the following normal form:

$$\dot{x} = \alpha_1 + \alpha_2 x - x^3 \quad (11)$$

Whereas for the *Andronov-Hopf bifurcation* the multidimensionality lies in the state, here it can be found in the two dimensional parameter $\alpha \in \mathbb{R}^2$. The state representation is one-dimensional, with state space $X \in \mathbb{R}$.

Visualization of the bifurcation surface

In order to visualize the bifurcation surface, one needs to plot all states, as configurations c where the derivative \dot{x} equals zero:

$$c \in \{(\alpha_1, \alpha_2, x) \mid \dot{x} = \alpha_1 + \alpha_2 x - x^3 = 0\} \quad (12)$$

¹<https://scipy.org/>

²<https://docs.scipy.org/doc/scipy/reference/generated/scipy.integrate.odeint.html>

³<https://computing.llnl.gov/projects/odepack>

Solving this condition for α_1 , we can calculate all values α_1 that satisfy the set condition (12) given a tuple of values (x, α_2) :

$$\alpha_1 = f(x, \alpha_2) = x^3 - \alpha_2 x \quad (13)$$

We use this method in a three step process to generate our 3D bifurcation plot.

1. Sample points (x, α_2) uniformly.
2. For each pair of points, calculate the corresponding value for α_1 that satisfies the steady-state condition (13).
3. Use this triplet of points to generate a 3D plot showing the bifurcation surface.

The figure below shows the resulting bifurcation plot, where the cusp can be observed at the front-side of the plot. If one imagines configuration settings (α_1, α_2) as vertical lines on the plot, one can see that the number of intersection points of this vertical configuration-line with the 3D bifurcation plot, (which are then equivalent to steady states in x for a given parametrization (α_1, α_2)), changes depending on the chosen configuration (α_1, α_2) of the system. For configurations that lie within the cusp, there are three steady states, while regions outside the cusp result in only one steady state. The bifurcation is happening at the borders of the cusp area. The cusp area, as a set of tuples (α_1, α_2) , can be visually identified by looking at the borders of the cusp when observing the top-view of the bifurcation plot. This view is shown in figure 4b.

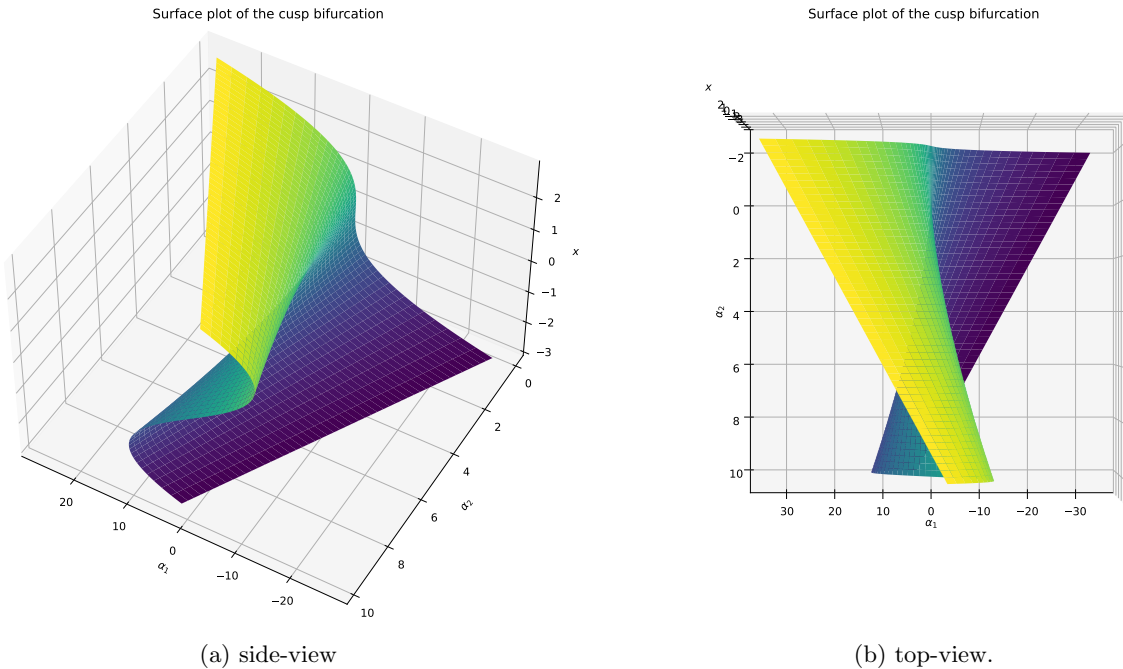


Figure 4: Bifurcation surface of *cusp bifurcation* as the set of all points (x, α_1, α_2) where $\dot{x} = 0$.

Report on task 4/5: Chaotic dynamics

Notebook: `task_4.ipynb`

Code: `helpers/math.py`, `helpers/plots.py`

Motivation

The aim of this task is to get first insights about chaotic system theory. This field of study plays a fundamental role in various scientific disciplines such as fluid mechanics, control technology, but also in the analysis of crowds. Chaos is defined as the high sensitivity of systems to changes in starting conditions and parameters. For this purpose, the behaviour of two non-linear dynamic systems is evaluated. In discrete space, the parameter dependence of the Logistic Map is analyzed. In continuous space, on the other hand, the disproportionate influence of small changes in the initial conditions is demonstrated using the Lorenz system. This chapter examines the Logistic Map in the first section and the Lorenz System in the second.

Logistic map

The logistic map is a map discretized in time derived from the first-order differential equation of the logistic equation. The parameter that significantly determines the behaviour can be interpreted as the growth rate r of a population. The iterative variable X indicates the population. Equation (14) establishes a relationship between the current population x_n and the population lying one time step in the future x_{n+1} .

$$x_{n+1} = rx_n(1 - x_n), \quad n \in \mathbb{N} \quad (14)$$

Methodology

In the following section, the logistic map will be examined more closely for bifurcations and steady states. Since negative populations occur for $r > 4$ and the population ratio x also leaves the interval $[0, 1]$, only the interval $r \in (0, 4]$ will be considered in the following. The aim of this sub-task is to find out whether there is a dependence on the initial population x_0 and whether there are interval limits of the growth parameter at which behavioural characteristics of the system appear. Since there is no information about the limit values and step sizes available, an analytical inspection from Equation (14) could deliver first hints. Subsequently, these analytically determined interval limits need to be confirmed experimentally.

Analytical Assumptions

A steady state is found if the population in x_{n+1} is equal to the population of the previous time step x_n . Graphically, this means that all points on which the future and current population is constant lie on a straight with $y = x$ and the slope $m = 1$ since the ratio of the populations has to equal to one. Plotting different growth rates and this straight line into one plot, one can see that there are intersections of the graphs for certain r . Such a plot is shown for the first interval in Figure 5.

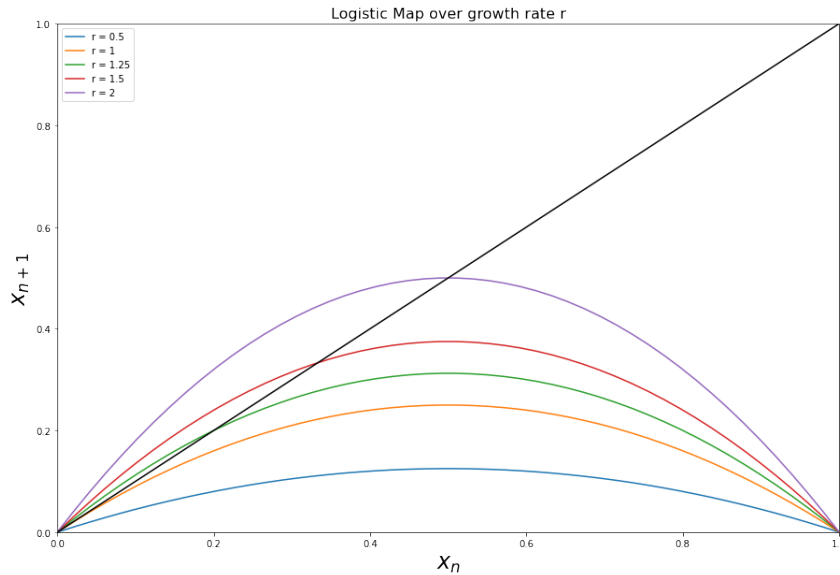


Figure 5: Shows the ratio of x_{n+1} and x_n with the logistic map from Equation (14) function for various r

By analyzing the number of intersection points, one can find that for all $r \in (0, 1]$ there is only one intersection point in the origin. Additionally, one can find a second intersection point of the parabola with the straight for certain r . The second intersection point only exists for $r > 1$ and is located at $x_n = 1 - \frac{1}{r}$.

This can also be shown analytically by converting Equation (14) into the following equation:

$$0 = rx_n(x_n - 1 + \frac{1}{r}), \quad n \in \mathbb{N} \quad (15)$$

Analyzing the null product, one can obtain the two steady states (=intersections of straight with parabola) in $x_{01} = 0$ and $x_{02} = 1 - \frac{1}{r}$. Now that the location of the fix points is known, stability is still of interest. For this, one can analyze the derivative function of the logistic map function in the fix points. According to [7] a point is stable if $|f'(x^*)| < 1$ where x^* is the fix point of a system. Complementary it is unstable when $|f'(x^*)| > 1$.

Applied to the logistic map one receives:

$$f'(x_n) = r(1 - 2x_n), \quad n \in \mathbb{N} \quad (16)$$

By evaluation the slope in the fix points one can find that $f'(x_{01} = 0) = r$ and $f'(x_{02} = 1 - \frac{1}{r}) = 2 - r$.

Since we are only interested in the absolute value of the slope one can derive that $|f'(x_{01} = 0)| = |r| < 1$ for all $r < 1$. This means that all $r \in (0, 1]$ have a stable equilibrium in $x_{01} = 0$ and for all $r > 1$ this fix point becomes unstable.

Following the same reasoning, one obtains for the second fixed point $|f'(x_{02} = 1 - \frac{1}{r})| = |2 - r| < 1$ for all $1 < r < 3$. So one can conclude that for all $r \in [1, 3]$ the second fix point is stable and for all $r > 3$ unstable.

Since there is one change in stability it could be assumed that there is a bifurcation point in $r = 1$ which is a *Transcritical bifurcation*.

Behaviour Analysis: First Interval $r \in (0, 2]$

The table in 6 shows ten population generations over uniformly sampled growth rates r in the interval $(0, 2]$ with stepsize $\Delta r = 0.2$. It quickly becomes apparent that the previous assumption holds and that the behaviour changes depending if r is smaller or larger than one. For all $r \in (0, 1]$, the steady state seems to be $x_{01} = 0$, while for all $r \in (1, 2]$ a convergent behaviour towards $x_{02} = 1 - \frac{1}{r}$ emerges. This is also consistent with the analytical investigation of the system, since the steady state seems to be independent of the variable x_n .

Gen \ r	0,2	0,4	0,6	0,8	1	1,2	1,4	1,6	1,8	2
1	0,018	0,036	0,054	0,072	0,09	0,108	0,126	0,144	0,162	0,18
2	0,0035352	0,0138816	0,03065	0,053453	0,0819	0,115603	0,154174	0,197222	0,244361	0,2952
3	0,00070454	0,00535274	0,017827	0,040476	0,075192	0,122687	0,182566	0,253321	0,332367	0,416114
4	0,000140809	0,00212964	0,010505	0,031071	0,069538	0,129162	0,20893	0,302639	0,399419	0,485926
5	2,81578E-05	0,00085004	0,006237	0,024084	0,064703	0,134975	0,231389	0,337678	0,43179	0,499604
6	5,6314E-06	0,00033973	0,003719	0,018803	0,060516	0,140108	0,248988	0,357843	0,441625	0,5
7	1,12627E-06	0,00013584	0,002223	0,01476	0,056854	0,144573	0,26179	0,367666	0,443866	0,5
8	2,25255E-07	5,4331E-05	0,001331	0,011634	0,053622	0,148406	0,270558	0,37198	0,444328	0,5
9	4,50509E-08	2,1731E-05	0,000797	0,009199	0,050746	0,151658	0,276299	0,373778	0,444421	0,5
10	9,01018E-09	8,6922E-06	0,000478	0,007291	0,048171	0,15439	0,279941	0,374509	0,444444	0,5
x0	0,1									

Figure 6: Table of the first ten generations for the logistic map equation for the interval $r \in (1, 2]$ with a step size of $\Delta r = 0.2$. Similar values are highlighted with related colours. One can clearly see that all values for all $r < 1$ tend towards 0 (red), while from $r = 1$ on wards all values tend towards a limit value dependent on r (yellow to green).

This hypothesis can be further supported by displaying the orbit for different growth rates over $n=100$ generations. Furthermore, the evaluation of the orbits helps to understand if the convergence behaviour depends on the initial population value x_0 . An excerpt of such an analysis is displayed in Figure 7 where Figure 7a shows the trajectory of for the initial population value $x_0 = 0.1$ and Figure 7b for $x_0 = 0.9$. It becomes apparent that the trajectories seem to converge towards the same value after a few different correction iterations in the beginning.

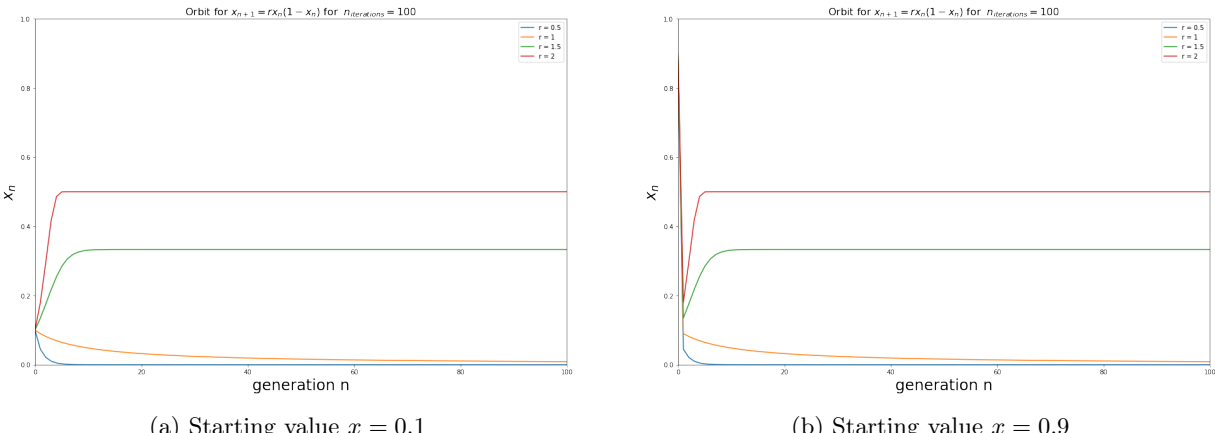


Figure 7: Shows the orbit and independence of the starting value x for four growth rates r sampled uniformly with a step size $\Delta r = 0.5$ within the first interval $r \in (0, 2]$

This is in line with the findings from the analytical evaluation of the system, according to which the slope and thus the stability of the system seems to be independent of the initial population in this interval.

Behaviour Analysis: Second Interval $r \in (2, 4]$

Equally to the previous section, the interval $r \in (2, 4]$ is examined by uniformly varying the growth rate r with a step size of $\Delta r = 0.2$. For all $2 < r < 3$ the development of the first ten generations seem to converge to the known steady state $x_{02} = 1 - \frac{1}{r}$. From the point $r = 3$ on, however, the behaviour of the system changes again. The previous steady state seem not to be stable anymore. This can be seen in Figure 8 from the colour highlighting in the table. At first glance, the values for this interval seem to behave arbitrarily, which is why for this interval a closer look at the orbits is required.

Gen \ r	2,2	2,4	2,6	2,8	3	3,2	3,4	3,6	3,8	4
1	0,198	0,216	0,234	0,252	0,27	0,288	0,306	0,324	0,342	0,36
2	0,3493512	0,4064256	0,466034	0,527789	0,5913	0,656179	0,722038	0,788486	0,855137	0,9216
3	0,500070866	0,5789852	0,647	0,697838	0,724993	0,721946	0,682378	0,600392	0,470736	0,289014
4	0,549999989	0,58502721	0,593816	0,590409	0,598135	0,642368	0,736911	0,863717	0,946746	0,821939
5	0,544500002	0,5826489	0,627116	0,677114	0,721109	0,73514	0,65917	0,423756	0,191589	0,585421
6	0,54564345	0,58360598	0,607988	0,612166	0,603333	0,623069	0,763861	0,879072	0,588555	0,970813
7	0,545416686	0,58322409	0,61968	0,664773	0,717967	0,751533	0,613283	0,382695	0,9202	0,113339
8	0,545462114	0,583377	0,612759	0,62398	0,607471	0,59754	0,806368	0,850462	0,27904	0,401974
9	0,545453032	0,58331586	0,616942	0,656961	0,71535	0,769555	0,530872	0,457835	0,764472	0,961563
10	0,545454848	0,58334032	0,614444	0,631017	0,610873	0,567488	0,84676	0,893599	0,684208	0,147837
x0	0,1									

Figure 8: Table of the first ten generations for the logistic map equation for the interval $r \in (2, 4]$ with a step size of $\Delta r = 0.2$. Similar values are highlighted with related colours. One can clearly see that all values for all $r < 3$ tend towards a limit value dependent on r (yellow). For all $r > 3$ irregular behaviour can be recognized (green, yellow, red).

Since the extract over the first 10 values suggests a change in the behaviour from $r=3$, parameters are to be evaluated uniformly around the event point in more detail. For this purpose, the orbit is considered over $n=100$ iterations in the interval from $r \in [2.8, 3.2]$.

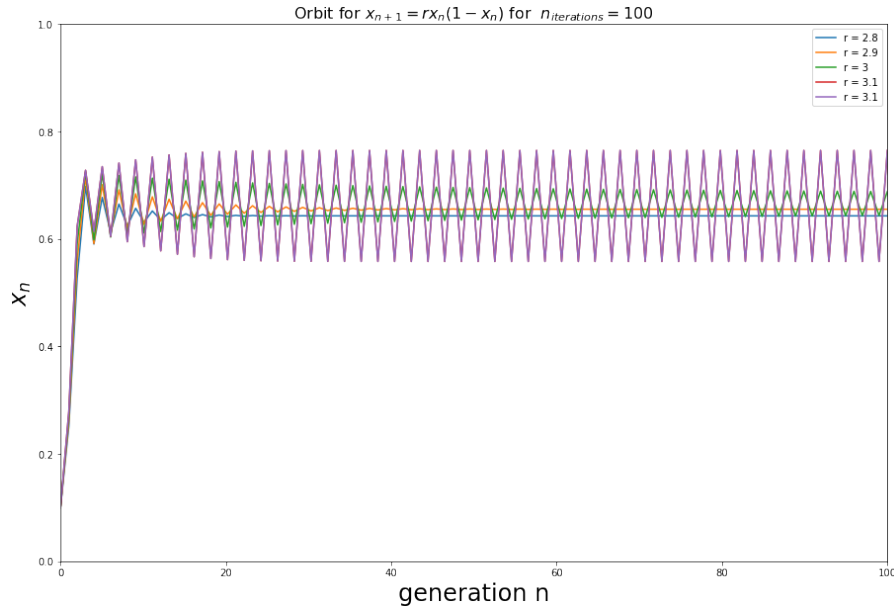


Figure 9: The figure shows the orbit for the growth rate values $r \in [2.8, 3.2]$ with a step size of $\Delta r = 0.1$. One can see that for all $r < 3$ that the amplitude is a damped oscillation converging against a value. At the larger amplitudes for $r > 3$ the amplitude seems to be constant and oscillates between a constant lower and upper boundary.

The Figure 9 shows that for the values $r < 3$ the amplitude of the oscillation decreases over time and thus the trajectory converges into a stable state. Thus it becomes clear that all trajectories in the interval $r \in [2, 3]$ run alternately against the previously calculated stability point into $x_{02} = 1 - \frac{1}{r}$. However, a different behaviour appears for all values $r > 3$. Here it seems as if the orbit builds up in the initial iterations and then oscillates back and forth between two accumulation points. The only surprise here is the view of the last four columns in 8, as they no longer correspond to previous value patterns. In order to examine this phenomenon more closely, the orbit for these values should be investigated.

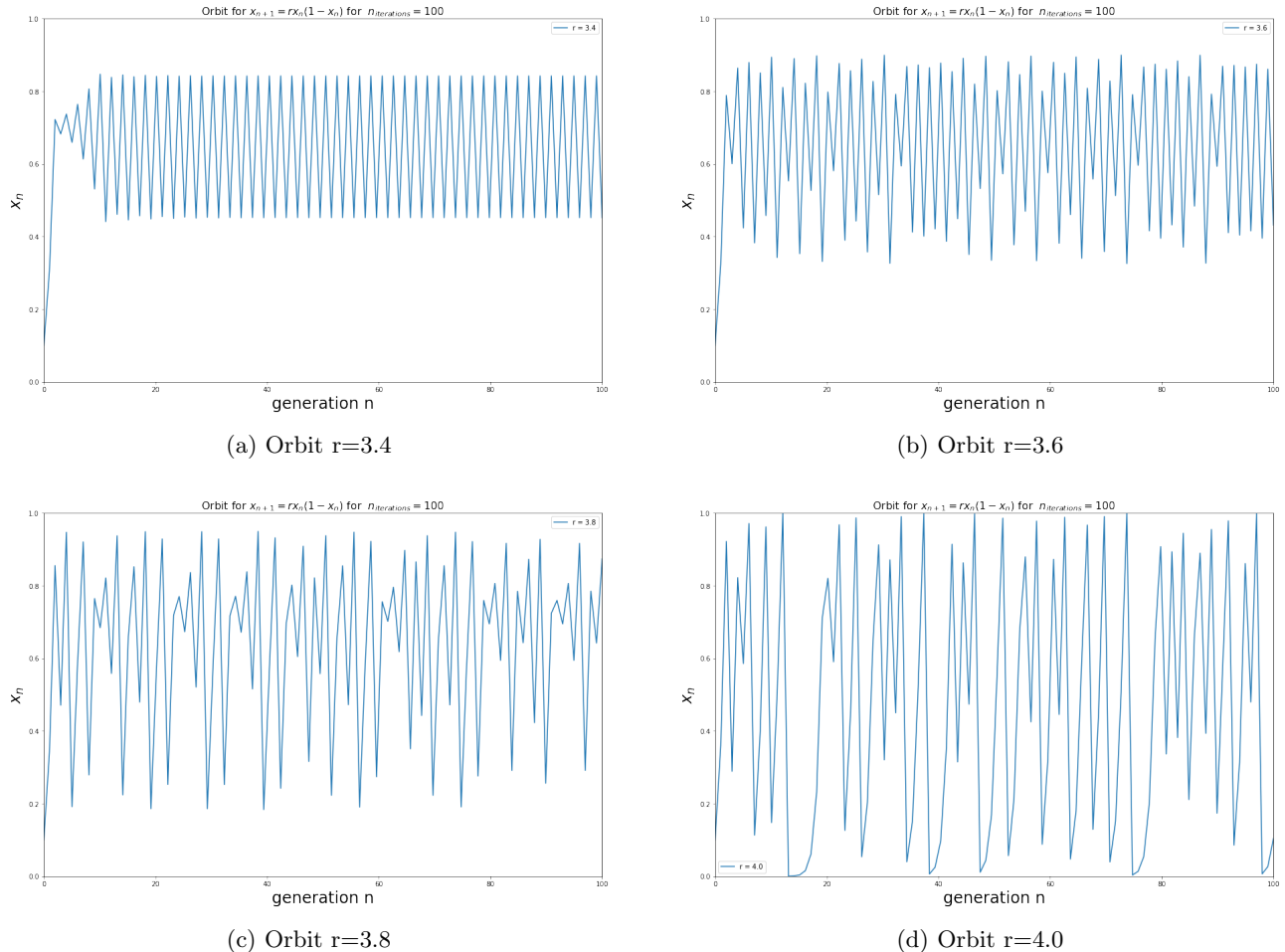


Figure 10: The figure shows the orbits for the growth rate values $r \in [3.4, 4.0]$ with a step size of $\Delta r = 0.2$. One can see that there is only for $r = 3.4$ an amplitude which oscillates between a constant lower and upper boundary. The remaining orbits do not seem to follow a clear pattern. The oscillations seem arbitrary.

Figure 10 illustrates the temporal course of the amplitudes for the last four columns in table 8. It becomes apparent that the orbit for $r = 3.4$ shows the usual pattern with the two accumulation points. However, it is surprising that the behaviour changes again for the remaining r values. The system falls into a state of chaos. A further refinement of the observation step size makes it possible to recognise that this chaotic behaviour occurs from the point $r=3.57$ onwards. Not shown in order not to go too far beyond the scope of the submission.

In order to get an idea of the influence of the initial value on the periodic system behaviour in this interval, one can compare the graphs for an $r < 3.57$ and one for $r > 3.57$ for two initial values $x_0 = 0.1$ and $x_0 = 0.5$. This leads to the impression that for many iterations there is no influence on the periodic development for $r < 3.57$. For $r > 3.57$ it seems like the courses differ. This behavior is of course in line with the observation that chaotic systems (which exist from $r = 3.57$ onwards) react very sensitively to changes in initial conditions.

Bifurcation Analysis

All observations from the previous section can also be read from the bifurcation diagram. For this reason, the stable populations were plotted against the growth rate r for $n=1000$ generations. Figure 11 shows the bifurcation diagram in the interval of the growth rate $r \in (0, 4]$.

The flat line along the zero line shows that for all growth rates $r \in (0, 1]$ the population dies out independently of the initial population x_0 . This changes at the bifurcation point $r = 1$ (*Transcritical bifurcation*). From this point onwards a stable equilibrium (= stable population level) always settles down until we reach $r = 3$ (*Period Doubling bifurcation*). The behaviour is consistent with the observations for the orbits since in this interval the amplitude decreases over time and converges towards the second steady state $x_{02} = 1 - \frac{1}{r}$.

For all $r \in [3, 3.54)$, two accumulation points arise in the orbit. In the bifurcation diagram, this is recognisable by the spreading of the graph into two lines from this point, so that there can be two population levels for the same growth parameter. From this point one can find a doubling of the accumulation points for all $r \in [3, 3.57)$.

From the point $r = 3.57$ on, the system falls into chaos, which is also clearly recognisable in Figure 11 from the expansion of the blue area on the right side of the graph. In addition to the detailed orbit observation, the whole bifurcation diagram now reveals that there still seems to be cluster points for certain parameter constellations for which we can again find a fixed number of accumulation points. These can be recognised by the white lines in the detailed view in Figure 12. For example, in the region around $r=3.82$ there are first 3 then 6 cluster points.

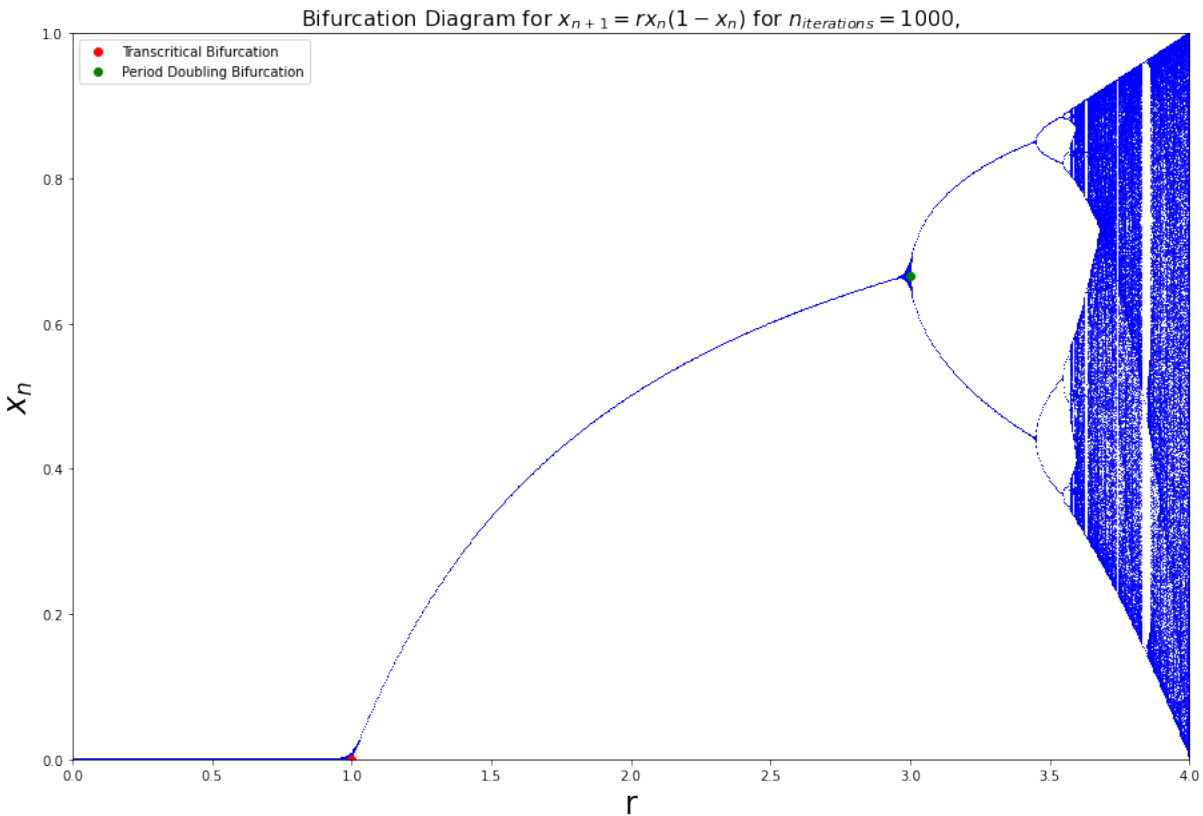


Figure 11: Total bifurcation diagram for $r \in (0, 4]$ for $n = 1000$ iterations

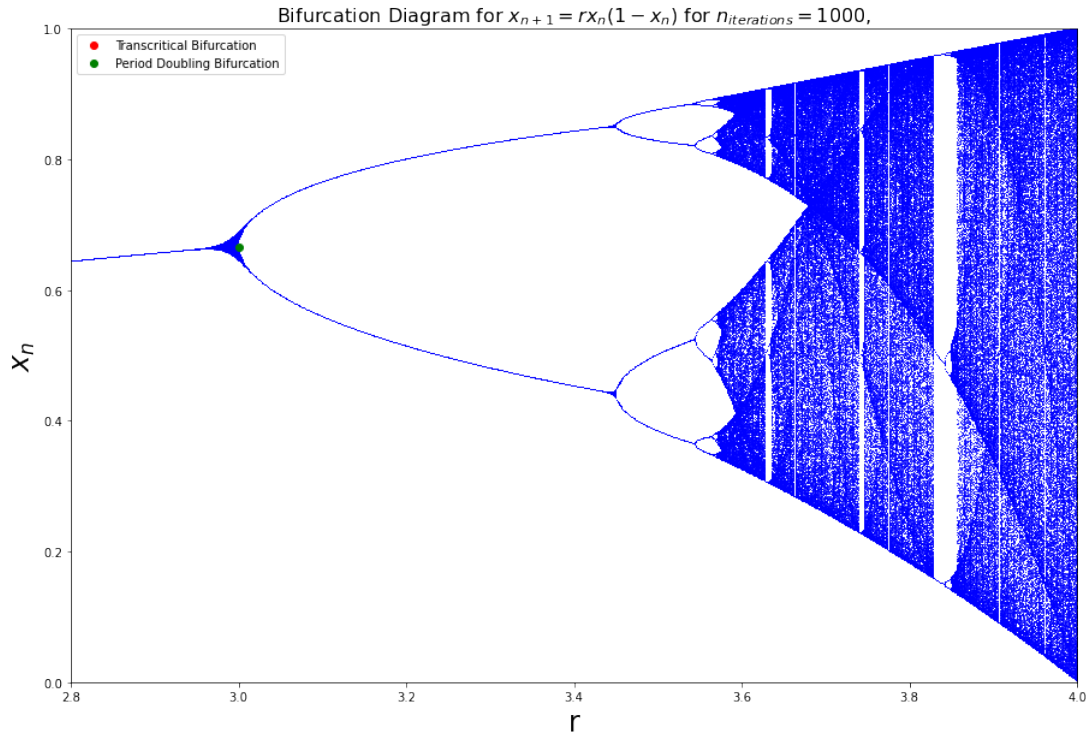


Figure 12: Detail breakout of the bifurcation diagram for $r \in [2.8, 4]$ for $n = 1000$ iterations

Result overview part I

This exercise has shown that the bifurcation diagram provides a lot of information about a dynamic system in a very compact form. Observations made on the basis of laborious calculations or orbit analyses can be read much more efficiently from the bifurcation diagram. The following is a brief summary of the results:

1. **Interval $r \in (0, 1]$:**
stable steady state in $x_{01} = 0$, result independent of initial population X_0 , for $n \rightarrow \infty$ population dies (at $r=1$ *Transcritical bifurcation*)
2. **Interval $r \in (1, 2]$:**
stable steady state in $x_{02} = 1 - \frac{1}{r}$, result independent of initial population x_0 , for $n \rightarrow \infty$ population survives with population level of $1 - \frac{1}{r}$
3. **Interval $r \in (2, 3]$:**
stable steady state in $x_{02} = 1 - \frac{1}{r}$, result independent of initial population X_0 , for $n \rightarrow \infty$ population survives with population level of $1 - \frac{1}{r}$ (in contrast to the previous interval this state is arrived by an alternating damped amplitude)
4. **Interval $r \in (3, 3.57]$:⁴**
for $n \rightarrow \infty$ population survives, instable population level (see fork in bifurcation diagram), result independent of initial population X_0 , this interval is characterised by the period doubling of the orbits (see [2] for detailed boundary setting within this interval)
5. **Interval $r \in (3.57, 4]$:**
for $n \rightarrow \infty$ population survives, chaotic behaviour of the system (= multiple possible population level for one growth parameter r), result dependent of initial population X_0 , for certain parameter constellations there could be fixed number of accumulation points of orbits again (see white areas in the interval)

⁴https://en.wikipedia.org/wiki/Logistic_map

Lorenz attractor

The Lorenz system is the name given to the three ordinary differential equations derived from Lorenz equations. Equation (17) show these. The Lorenz attractor is the subset of parameters for which the Lorenz System shows chaotic behaviour. A possible example of such a parameter combination is given by $\sigma = 10$, $\beta = \frac{8}{3}$ and $\rho = 28$. For this parameter set the lorenz attractor can be categorised as a strange attractor.

$$\begin{aligned}\dot{x} &= \sigma(y - x) \\ \dot{y} &= x(\rho - z) - y \\ \dot{z} &= xy - \beta z\end{aligned}\tag{17}$$

Behaviour analysis

By visualizing a single trajectory starting at $x_0 = (10, 10, 10)$ one can get an understanding of the behaviour. The result is a shape like a lying eight. The holes (limit cycles) of this shape are orbited in many irregular paths resulting in irregular variation of perimeters over time. The orbits do not show a fixed pattern i.e. the motion of the system does not seem to repeat itself periodically. If one compare two points with each other, one can see that they might be close to each other at one time but are arbitrarily far away from each other at later times. At certain times, when the distance to a center is large enough, the trajectory seems to leave the orbit of one hole, but is directly attracted by the other hole. This process occurs several times during the simulation. It therefore seems as if the attractor is globally stable in itself, i.e. the trajectory cannot leave this shape at any time, but always orbits around one of the two holes. Nevertheless, there must be a local instability that makes the hole change possible at certain points in time.

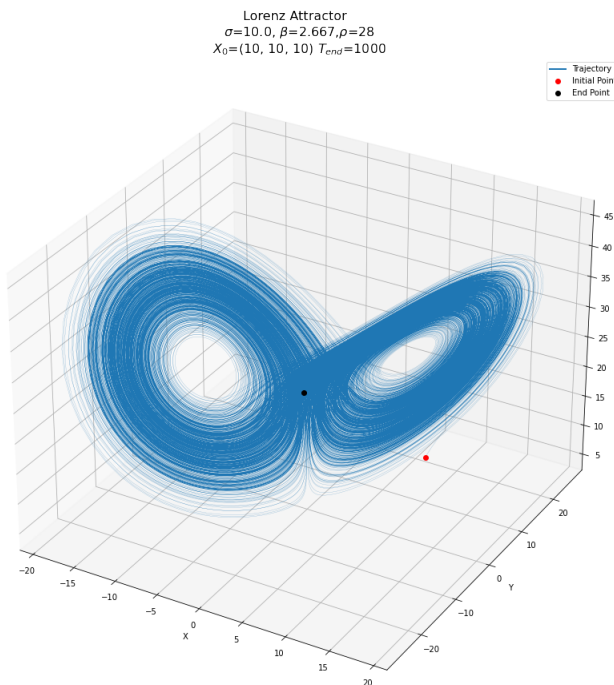


Figure 13: Illustrates the Lorenz Attractor for the first parameter set (details in the plot title). The blue line is a single trajectory. The red dot shows the initial value and the black one the last state for simulated range.

Initial condition dependence - first parameter set

As already described in the introduction to this task, the Lorenz attractor is often associated with the butterfly effect. This states that even small changes in the initial conditions can lead to large changes of subsequent states. For this purpose one can visualize a second trajectory $\hat{x} = (10 + 10^{-8}, 10, 10)$ with a very small offset to the first at $x_0 = (10, 10, 10)$. It becomes apparent that the two orbits of the system differ disproportionately to the very small change at the beginning. This becomes particularly visible when you compare the black endpoints in the two orbit plots with each other.

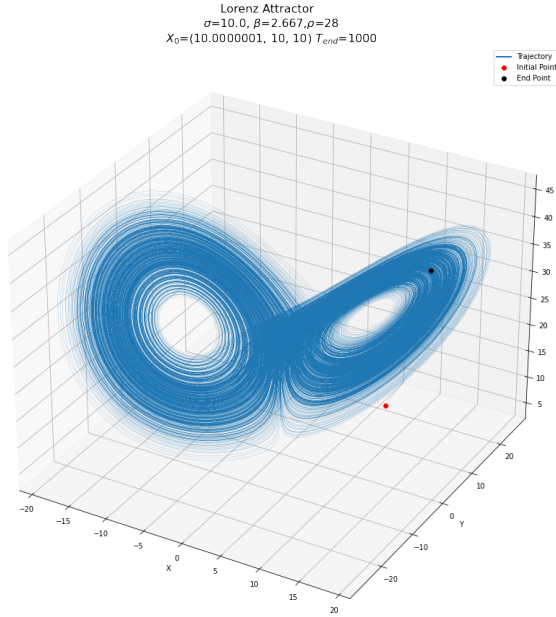


Figure 14: Illustrates the Lorenz Attractor for the first parameter set (details in the plot title), but for a small offset of the starting position. The blue line is a single trajectory. The red dot shows the initial value and the black one the last state for simulated range.

It becomes even clearer if you compare the states over time with a distance metric like the L2-Norm where $d = \|x(t) - \hat{x}(t)\|_2$. The resulting distance for the simulated time of $T_{end} = 1000$ is shown in Figure 15. The threshold value of $d \geq 1$ is exceeded for the first time in the iteration $n=2035$ which corresponds to $t = 20.35$ simulated seconds.

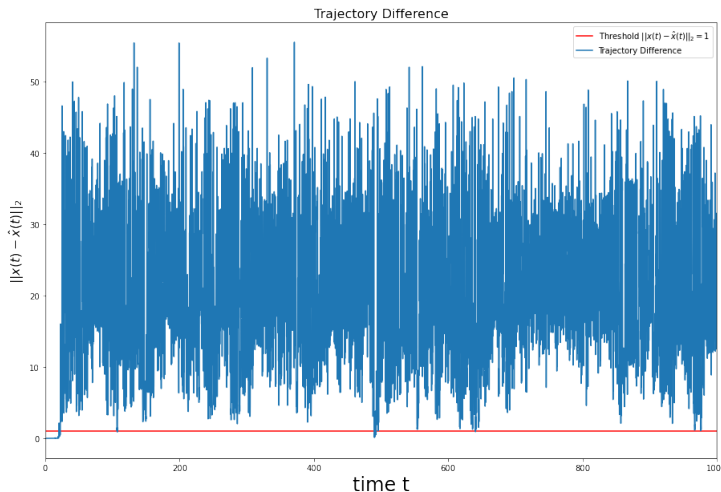


Figure 15: Distance values over the simulated range. The red line indicates the threshold of $d=1$.

Initial condition dependence - second parameter set

That the sensitivity to initial conditions is highly dependent on the chosen parameter set should be shown in this section. Therefore the parameter ρ should be changed to $\rho = 0.5$ and then the experiment should be carried out again with all other parameters remaining the same. The resulting orbits in 3D are illustrated in Figure 16. Compared to the previous experiment, the course of the trajectories and endpoints seem to be the same.

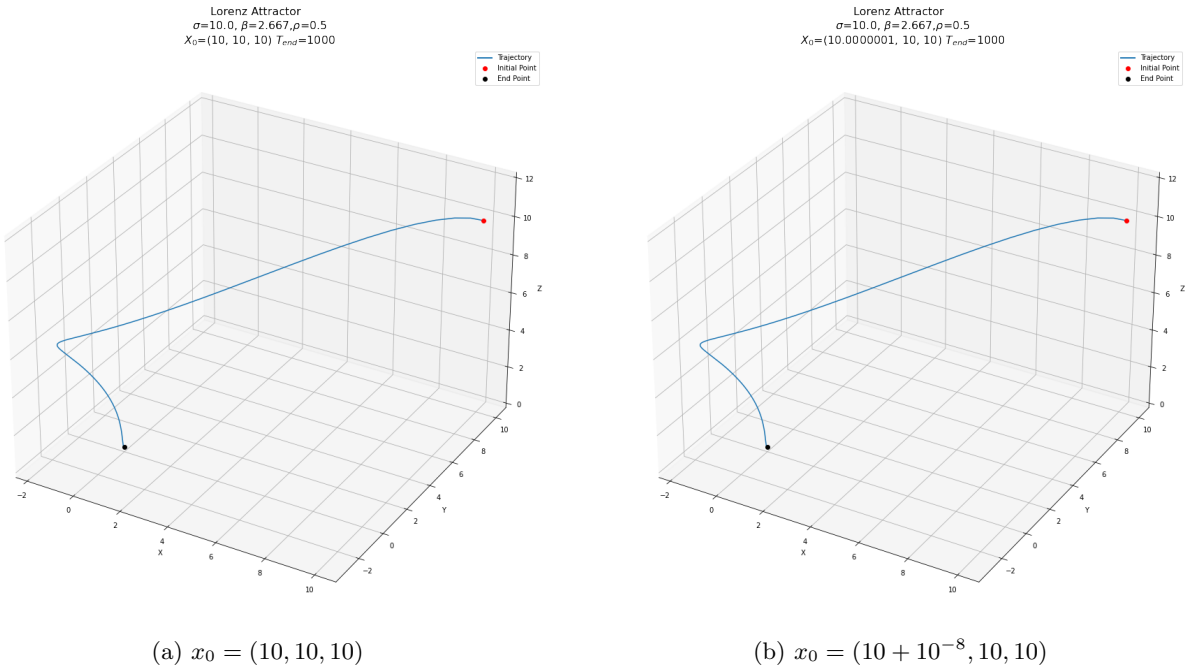


Figure 16: Illustrates two 3D orbits of the Lorenz system for the second parameter set and two different starting values.

To be sure, one can again look at the L2 norm about the difference of the two trajectories over time. In detail, Figure 17b shows that the small offset tends towards zero within the first three iterations. Moreover, Figure 17a shows that there is no noticeable difference of the two courses. The result above indicate that there is a stable fix point of the Lorenz system in the origin $X = (0, 0, 0)$ for the selected parameter constellation. This implies that there are states of the system in which the initial value change does not lead to the large distortions of subsequent states.

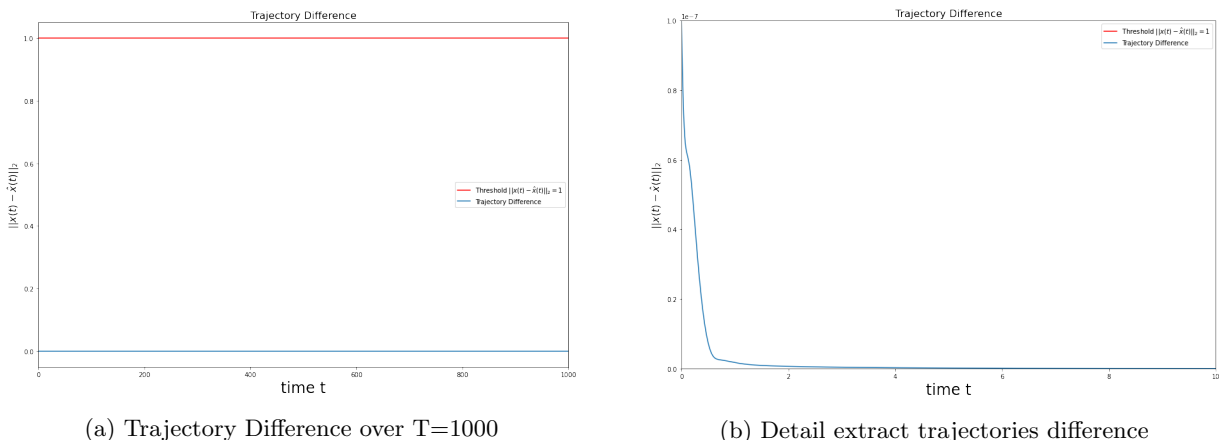


Figure 17: Distance values over the simulated range. The red line indicates the threshold of $d=1$.

Bifurcation Analysis

In this section, the previously found hypothesis that there are different states of the system will be examined more closely. The comparison of the two experiments has already shown that there must be at least one bifurcation in the interval $\rho = [0.5, 28]$, since for $\rho = 0.5$ a stable fixed point seems to exist, whereas for $\rho = 28$ the picture of the lying eight with the two limit cycles shown in Figure 13 arises. Of course, this now raises the question of whether only one or several bifurcations exist and where the bifurcation points are located.

In order to systematically determine the dependence of the stability of the system on the parameter ρ , one can determine fix points analytically or experimentally. Due to the existence of the programmed framework with which one can evaluate the orbit in 3D as well as the orbit over time, these points are to be determined experimentally in the following. Due to the limited time and resources, this was then supplemented with a similarly conducted experiment from the literature.

To represent as many different states of the system as possible with the smallest possible number of necessary plots, 6 images of the 3D orbit were calculated and visualised starting from the point $\rho = 1$ with a step size of $\Delta\rho = 5$. These were then placed in the corresponding position in the bifurcation diagram from [3] on the basis of their ρ value. A fusion of the bifurcation diagram and the corresponding 3D orbit plots is shown in Figure 18. The same procedure can be used for the orbit over time, as the convergence behaviour can be seen even more clearly here. This is illustrated in Figure 19.

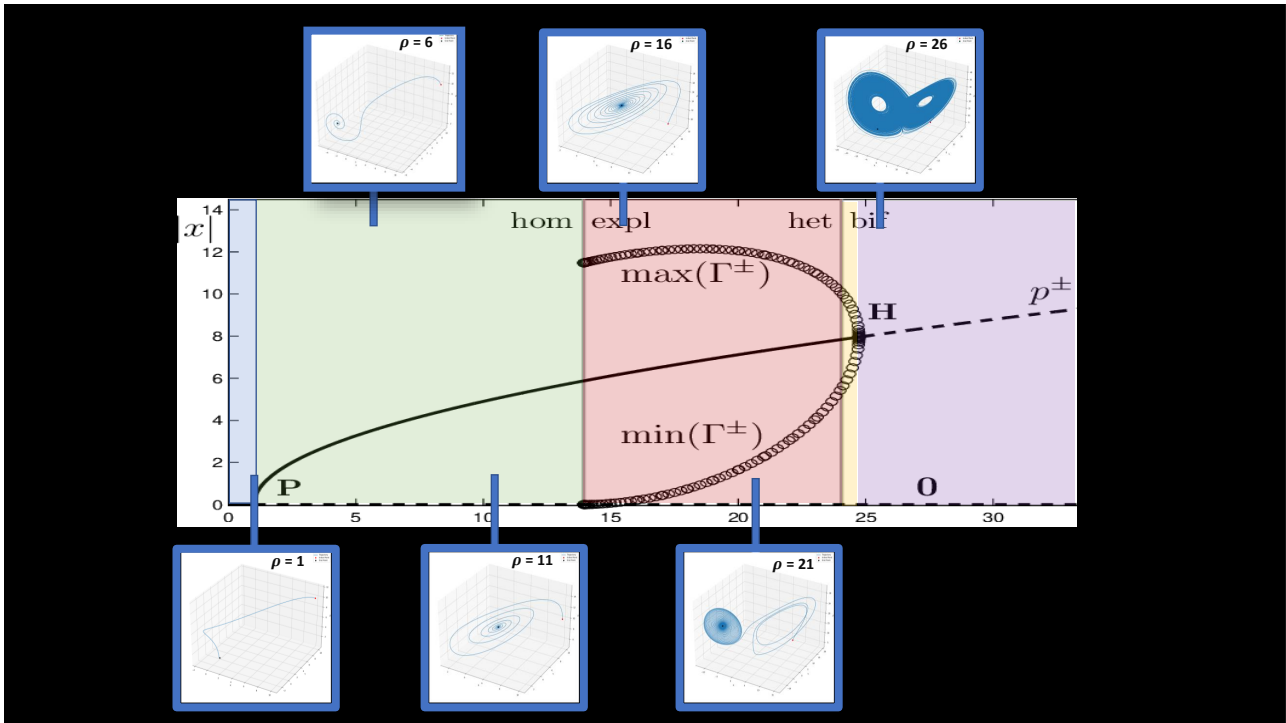


Figure 18: The core of this figure is the bifurcation diagram over x (ordinate) and the parameter ρ (abscissa). The interval shown is $\rho \in [0, 35]$. This diagram is taken from [3]. In a post-processing step, the areas with the same stability were highlighted in different colours. Six 3D orbits calculated with our framework are shown around the bifurcation diagram. The blue line is used for classification on the abscissa according to the respective ρ value of the corresponding plot. For the sake of clarity, this is also marked again in the top right of the respective plot.

Using the bifurcation diagram, one can now see that a *Pitchfork bifurcation* exists for $\rho = 1$. This also allows to classify and interpret the result of our experiment for $\rho=0.5$ and confirms the assumption that for all ρ from this interval (highlighted in blue) the trajectory leads to the origin. In the temporal course of the orbit you can see this in the convergence towards zero.

The orbit plots created with $\rho = 6$ and $\rho = 11$ are both in the same stability interval (highlighted in green) and also show the same behaviour with different degrees of intensity. The behaviour can be described as a spiral around an end point that is not left again. Upwards, this interval is delimited by the *Homoclinic bifurcation* in $\rho=13.9265$. In the temporal course of the orbit, one can see that a damped amplitude occurs. Depending on the location within this interval, it tends towards different values at different rates.

The orbit plots created with $\rho = 16$ and $\rho = 21$ are also both in the same stability interval (highlighted in red), which is delimited by *Heteroclinic bifurcation* in $\rho = 24.0579$. The behaviour in this interval could be interpreted as transient chaos, because at the beginning it seems as if there are two points between which the trajectory will develop back and forth, but then over time a stable state emerges. This can be seen particularly well in the plot for $\rho=21$ with the two initial loops on the right side and the subsequent spiralling into the other fix point.

The yellow interval is the area between the *Heteroclinic bifurcation* and the *Hopf bifurcation* at $\rho = 24.74$. In this area a chaotic attractor and the two attracting equilibrium point co-exist. Over time one will end up in one of the two fix points. Due to the too long simulation time required and the clarity of representation, no plot was created for this minor interval.

The last interval considered is that for all ρ greater than the *Hopf bifurcation* in $\rho = 24.74$. This area is marked in purple. In this area only the strange attractor is present. In the orbit over time plot for $\rho = 26$, it is very clear that the amplitudes are irregular and have the same magnitude over all times, so that no convergence behaviour is visible.

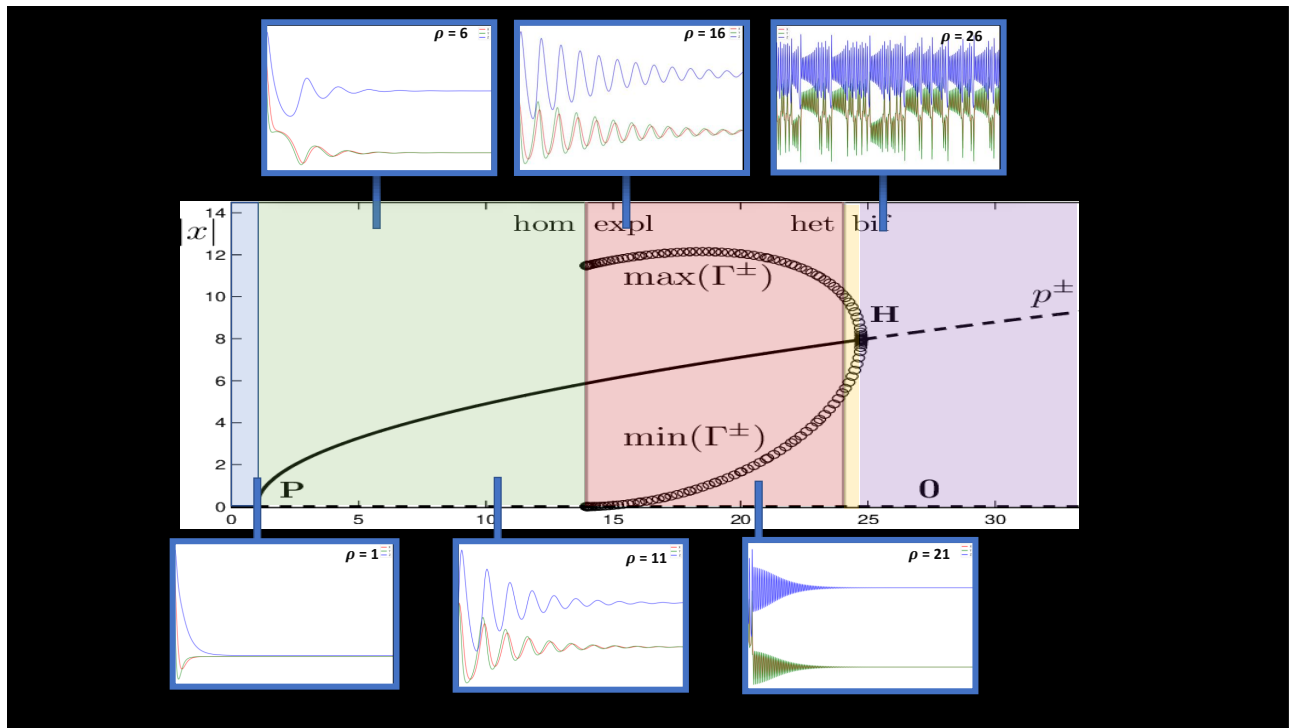


Figure 19: The core of this figure is the bifurcation diagram over x (ordinate) and the parameter ρ (abscissa). The interval shown is $\rho \in [0, 35]$. This diagram is taken from [3]. In a post-processing step, the areas with the same stability were highlighted in different colours. Six orbits over time were calculated with our framework which are shown around the bifurcation diagram. The blue line is used for classification on the abscissa according to the respective ρ value of the corresponding plot. For the sake of clarity, this is also marked again in the top right of the respective plot.

In conclusion, the interval of $\rho \in [0, 5, 28]$ to be investigated can be divided by four bifurcation points and hence into the five areas highlighted in colour.

Report on task 5/5: Bifurcations in crowd dynamics

Notebook: `task_5.ipynb`

Code: `helpers/sir.py`

Motivation

Bifurcations can be observed in almost every dynamical system. In particular, one is able to use bifurcation theory to analyse crowd systems like the SIR model where people can be either susceptible, infected or removed by recovery or death. The behaviour of such a system strongly depends on a variety of factors like recovery rates, death rates, and the resources of a health system. In this task, the health system is modelled by the number of available hospital beds because this has a high impact for fighting diseases. The dynamical system is defined and then analysed for different numbers of available beds in order to discover bifurcations. In addition to that, the existence of the *Hopf bifurcation*, the reproduction rate R_0 and the equilibrium state E_0 are presented.

Defining a differential equation based SIR model

In order to observe bifurcations for crowd dynamics, the SIR model of Shan and Zhu [5] is analysed. They define a system with the following differential equations:

$$\begin{aligned}\frac{dS}{dt} &= A - \delta S - \frac{\beta SI}{S + I + R} \\ \frac{dI}{dt} &= -(\delta + \nu)I - \mu(b, I)I + \frac{\beta SI}{S + I + R} \\ \frac{dR}{dt} &= \mu(b, I)I - \delta R\end{aligned}\tag{18}$$

with μ being the per capita recovery rate of infectious people and defined by

$$\mu(b, I) = \mu_0 + (\mu_1 - \mu_0) \frac{b}{b + I}\tag{19}$$

The meaning of the parameters and the values that are chosen for an analysis are described in 6.

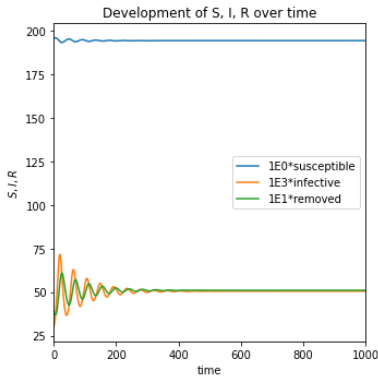
Name	Value	Definition
S	variable	number of susceptible people
I	variable	number of infected people
R	variable	number of removed people
A	20	recruitment/ birth rate of susceptible people
δ	0.1	per capita natural death rate
ν	1	per capita disease-related death rate
β	11.5	average number of contacts per time unit with infectious people
μ_0	10	minimum recovery rate
μ_1	10.45	maximum recovery rate
b	variable	number of hospital bed per 10000 individuals

Table 6: Definitions of the parameters of the SIR model with fixed or variable values

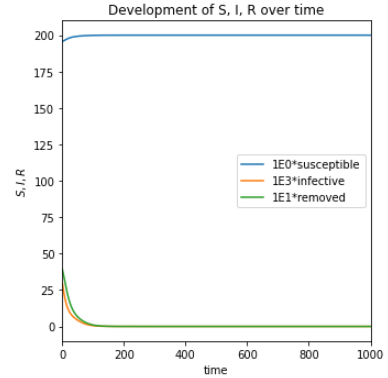
Analysing the system for different values of b

The system is analysed by changing the parameter b in small increments of 0.001 in the interval $I = [0.01, 0.03]$. Three starting points are chosen with different initial values of susceptible, infectious and removed individ-

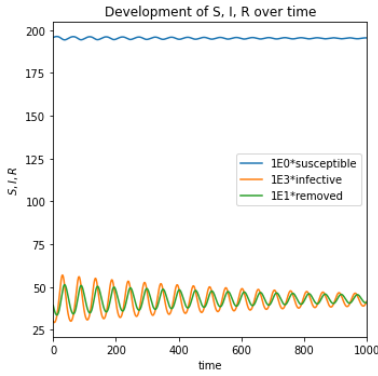
uals. The first point is $Sim_1 = (S_0, I_0, R_0) = (195.3, 0.052, 4.4)$, the second one is $Sim_2 = (S_0, I_0, R_0) = (195.7, 0.03, 3.92)$ and the third one is $Sim_3 = (S_0, I_0, R_0) = (193, 0.08, 6.21)$. While the parameter b is increased in small steps, the system is visualised by a 2D and a 3D plot that show the development of the numbers of susceptible, infected and removed people.



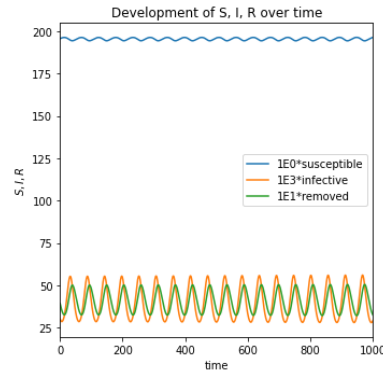
(a) $b = 0.015$: oscillations that reduce until a constant number of 50 infections and recoveries



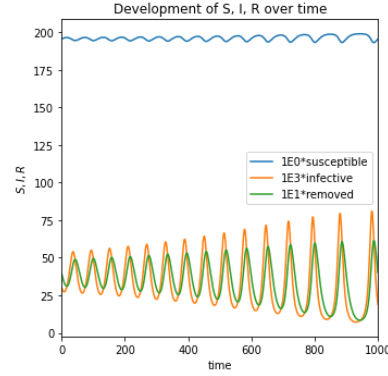
(b) $b = 0.030$: decreasing number of infections until the whole population is susceptible



(c) $b = 0.021$: oscillations of the S, I and R curves with decreasing amplitude



(d) $b = 0.022$: oscillations of the S, I and R curves with constant amplitude



(e) $b = 0.023$: oscillations of the S, I and R curves with increasing amplitude

Figure 20: 2D Plots of the SIR system for different values of b and the starting point Sim_1 : curves for the numbers of susceptible (blue), infected (orange), and removed (green) people over time.

Fig 20 illustrates the observations for different values of b and the starting point Sim_1 . We distinguish 5 cases. For $b << 0.022$ (e.g. $b = 0.015$), one is able to observe that the numbers of susceptible, infected and removed individuals oscillate with decreasing amplitude until a constant number of 50 people get infected and removed (see Fig 20a). For values that are slightly smaller than 0.022 (e.g. $b = 0.021$), the amplitude of the oscillations still get smaller but need a longer period of time (see Fig 20c). Furthermore, the maximum amplitude is smaller than before. If $b = 0.022$ the amplitude is constant (see Fig 20d). One is able to observe that the center of the oscillations is below 50. This means that, on average, fewer people are infected in the same period of time. Values that are slightly greater than 0.022 (e.g. $b = 0.023$) result in an increasing amplitude of the oscillations (see Fig 20e). If $b >> 0.022$ (e.g. $b = 0.030$), the number of infections decreases until no one gets infected and the whole population stays susceptible (see Fig 20b). These results are not only achieved for Sim_1 , but also for the other starting points. The differences are the time that is required until the system converges and the amplitude of the individual curves. However, the observable bifurcations happen at $b = 0.022$ for all three starting points.

The observable bifurcation for all three starting points is visualised in Fig 21. If $b < 0.022$, then all points spiral inwards to a weak focus. For values $b > 0.022$, the points are spiraling towards a limit cycle. When the values of b are further increased, they all move to $(S, I, R) = (200, 0, 0)$. In the case that $b = 0.022$, there is a

weak focus and a stable limit cycle. As a result, there is also an unstable limit cycle between the focus and the stable limit cycle. The trajectories of Sim_1 move towards the weak focus while the trajectories of Sim_2 move outwards and the trajectories of Sim_3 move inwards to the stable limit cycle.

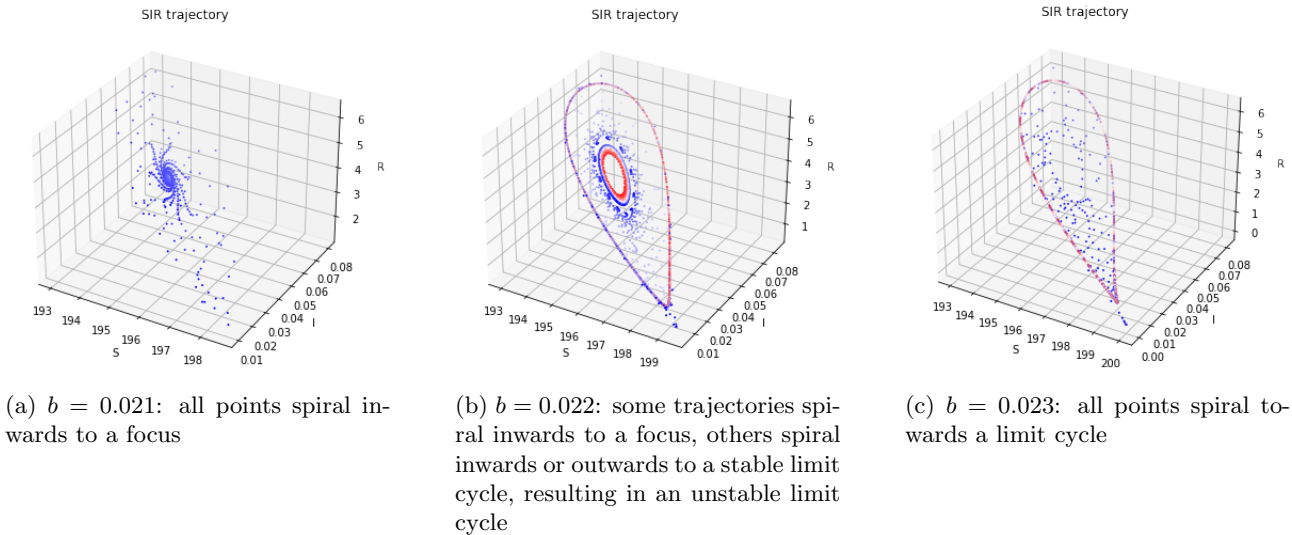


Figure 21: 3D Plots of the SIR system for different values of b and all three starting points: observations over time with blue indicating earlier states and red indicating subsequent states.

Hopf Bifurcation

Analysing the system for a Hopf bifurcation

The observable bifurcation at $b = 0.022$ is a *Hopf bifurcation*. A first indicator is that we receive a weak focus, a stable limit cycle and an unstable limit cycle. In order to prove this assumption, the results of [5] are used. Theorem 4.4 of [5, p.1674] states that we observe a *Hopf bifurcation* if $I_2 = H_m$, $I_2 = H_M$, or $I_2 = H_m = H_M$ where H_m and H_M refer to the positive roots of the indicator function $h(I)$ and I_2 is computed by the parameters of the system.

I_2 is defined by:

$$I_2 = \frac{-\mathcal{B} + \sqrt{\Delta_0}}{2\mathcal{A}} \quad (20)$$

$$\mathcal{A} = (\delta + \nu + \mu_0)(\beta - \nu) \quad (21)$$

$$\mathcal{B} = (\delta + \nu + \mu_0 - \beta)\mathcal{A} + (\delta - \nu)(\delta + \nu + \mu_1)b \quad (22)$$

$$\Delta_0 = (\beta - \nu)^2 \delta_1^2 b^2 - 2A(\beta - \nu)(\beta(\mu_1 - \mu_0) + \delta_0(\delta_1 - \beta))b + A^2(\beta - \delta_0)^2 \quad (23)$$

$$\delta_0 = \delta - \nu + \mu_0 \quad (24)$$

$$\delta_1 = \delta + \nu + \mu_1 \quad (25)$$

$h(I)$ is defined by:

$$\begin{aligned} h(I) &= c_3 I^3 + c_2 I^2 + c_1 I + c_0 \\ c_3 &= \delta(\beta - \nu) \\ c_2 &= (\mu_1 - \mu_0)b\nu + 2b\delta(\beta - \nu) + \delta A \\ c_1 &= b((\mu_0 - \mu_1 + 2\delta)A + (\beta - \nu)b\delta) \\ c_0 &= b^2 \delta A \end{aligned} \quad (26)$$

The results of the indicator function $h(I)$ are illustrated in Fig 22. For the given parameters, we receive an indicator function with two positive roots. The smaller root is defined as H_m and the bigger root as H_M .

The given parameters result in three roots of $h(I)$ ($[-2.010, 0.041, 0.011]$) and $I_2 \approx 0.041$. Because $H_m = 0.041$, we receive $I_2 \approx H_m$. Therefore the system presents a *Hopf bifurcation* at $b = 0.022$ according to [5].

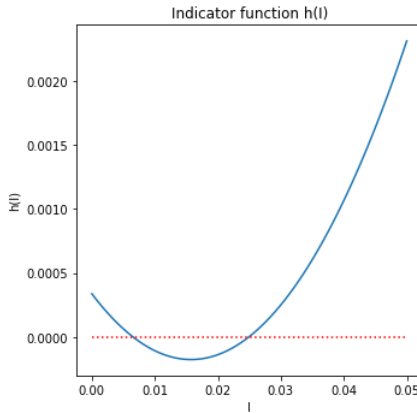


Figure 22: Indicator function $h(I)$ of the SIR system with 2 positive roots.

From our observations and Theorem 4.5 of [5], one is able to draw the conclusion that there is a weak focus, one stable and one unstable limit cycle from the *Hopf bifurcation*.

Normal Form of the Hopf Bifurcation

According to Kuznetsov [4, p.85], the normal form of the *Hopf bifurcation* is:

$$\dot{z} = (\alpha + i) * z - z * |z|^2 \quad (27)$$

where $z = x_1 + i * x_2$ and α is the parameter of the system.

Reproduction Rate R_0

When analysing the dynamics of the SIR model, an important factor that occurs is the reproduction rate R_0 . Shan and Zhu [5, p.1666] define R_0 in the following way:

$$R_0 = \frac{\beta}{\delta + \nu + \mu_1} \quad (28)$$

The reproduction rate R_0 depends on the number of infectious contacts β , the natural death rate δ , the disease-related death rate ν and the maximum recovery rate μ_1 . A small average number of contacts with infectious persons results in a small value for R_0 which will eventually eliminate the disease if it stays below $R_0 = 1$. The number of infected people will tend to 0. This is why it is particularly important to reduce one's contacts in order to reduce the number of contacts with infectious persons and therefore support an elimination of a disease. With a higher number of contacts with infectious persons, R_0 might exceed the threshold of 1 and the disease won't be stopped. The number of infected people will increase. While δ and ν are constants that cannot be changed in a short period of time, the other important factor is the maximum recovery rate that is based on the number of available beds in hospitals. Here, a high number of beds leads to a smaller R_0 . If only a few beds are available, R_0 will be higher.

Disease free equilibrium E_0

The reproduction rate R_0 can be used to determine the dynamical behaviours. Shan and Zhu [5] state that for different values of R_0 there can exist different equilibria. In addition to that, for $R_0 < 1$ there exists a attracting node at the disease free equilibrium $E_0 = (\frac{A}{\delta}, 0, 0)$. This equilibrium is a state where the whole population is susceptible and the number of infections and recoveries is zero. The effects of these results can also be observed

in our system with $E_0 = (200, 0, 0)$. In particular, for $b > 0.022$ all trajectories move towards E_0 . This means that the disease will be eliminated for $R_0 < 1$ and the given starting points. Values of (S, I, R) that are close to E_0 will lead to a state where all people are susceptible and no further infections will happen. This coincides with reality where diseases will be stopped if the reproduction rate is small and there are only a few people infected in the beginning.

Summary

In this task it is shown that one is able to apply bifurcation theory on dynamical systems like the SIR model. In our case, we only tuned the number b of available hospital beds, but it is also possible to change other parameters like the maximal recovery rate μ_1 and the average number of contacts with infectious people β . Shan and Zhu [5] present that analysing the dynamics of the model for different values of the triple of (μ_1, b, β) leads to the best results. Anyhow, we show that for the given parameters and $b = 0.022$, one is able to observe the *Hopf bifurcation* for the SIR model. With its normal form it is possible to derive how the system evolves over time.

References

- [1] Saddle-node bifurcation. https://en.wikipedia.org/wiki/Saddle-node_bifurcation. Accessed: 2021-12-04.
- [2] Dynamical systems - course me406. <http://www2.me.rochester.edu/courses/ME406/webexamp6/logistmap.pdf>, 2009. Accessed: 2021-12-04.
- [3] Hinke M. Osinga Eusebius J. Doedel, Bernd Krauskopf. Global bifurcations of the lorenz manifold. 2006.
- [4] Yuri A. Kuznetsov. Elements of applied bifurcation theory. 2004.
- [5] Chunhua Shan and Huaiping Zhu. Bifurcations and complex dynamics of an sir model with the impact of the number of hospital beds. *Journal of Differential Equations*, 257(5):1662–1688, 2014.
- [6] Philipp Städter, Yannik Schälte, Leonard Schmiester, Jan Hasenauer, and Paul L. Stapor. Benchmarking of numerical integration methods for ode models of biological systems. *Scientific reports*, 11(1):2696, 2021.
- [7] D. Serletis William Barnett, A. Serletis. Nonlinear and complex dynamics in economics. page 1773ff., 2014.